BIOCHEMISTRY
including biophysical chemistry & molecular biology

Article

pubs.acs.org/biochemistry

Inhibition and Allosteric Regulation of Monomeric Phosphoenolpyruvate Carboxykinase by 3-Mercaptopicolinic Acid

Marc D. Balan,[‡,§] Matthew J. Mcleod,[†] William R. Lotosky,[†] Mark Ghaly,[†] and Todd Holyoak*[,‡,†]

[†]Department of Biology, University of Waterloo, Waterloo, ON N2L 3G1, Canada

[‡]Department of Biochemistry and Molecular Biology, The University of Kansas Medical Center, Kansas City, Kansas 66160, United States

ABSTRACT: For almost 40 years, it has been known that tryptophan metabolites and picolinic acid analogues act as inhibitors of gluconeogenesis. Early studies observed that 3-mercaptopicolinic acid (MPA) was a potent hypoglycemic agent via inhibition of glucose synthesis through the specific inhibition of phosphoenolpyruvate carboxykinase (PEPCK) in the gluconeogenesis pathway. Despite prior kinetic investigation, the mechanism of the inhibition by MPA is unclear. To clarify the mechanism of inhibition exerted by MPA on PEPCK, we have undertaken structural and kinetic studies. The kinetic data in concert with crystallographic structures of PEPCK in complex with MPA and the substrates for the reaction illustrate that PEPCK is inhibited by the binding of MPA at two discrete binding sites: one acting in a competitive fashion with PEP/OAA (~10 μM) and the other acting at a previously unidentified allosteric site (K_i ~ 150 μM). The structural studies suggest that binding of MPA to the allosteric pocket stabilizes an altered conformation of the nucleotide-binding site that in turn reduces the affinity of the enzyme for the nucleotide.

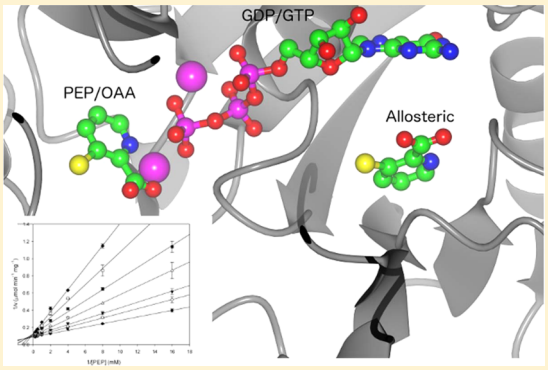

PEPCK catalyzes the reversible decarboxylation and phosphorylation of oxaloacetate (OAA) forming phosphoenolpyruvate (PEP), CO_2, and GDP. Historically, the primary role of the enzyme in almost all organisms has been proposed to be the formation of PEP in the first committed step of gluconeogenesis and glyceroneogenesis.[1] As such, PEPCK has a key role in highly gluconeogenic tissues such as liver and kidney, converting lactate and other precursors to glucose and releasing the sugar into the bloodstream. More recent studies suggest a role for PEPCK in other diverse processes like longevity and aerobic capacity.[2,3] Additional roles for PEPCK are also pointedly illustrated by both the observation that brown adipose tissue, which does not make glucose, has more PEPCK protein than the liver[4] and that PEPCK has a role in insulin secretion in the pancreas.[5] An essential role for PEPCK in the pathogenicity of *Mycobacterium tuberculosis* has also been recently illustrated, suggesting that PEPCK may represent a novel drug target for that organism.[6]

For almost 40 years, it has been known that tryptophan metabolites and picolinic acid analogues act as inhibitors of gluconeogenesis.[7−10] Early studies observed that 3-mercaptopicolinic acid (MPA) is a potent hypoglycemic agent that acts by inhibiting glucose synthesis. Additional kinetic studies with rat cytosolic PEPCK suggested that MPA specifically inhibits PEPCK in the gluconeogenesis pathway with a K_i of approximately 2−9 μM.[11] From these studies, it was hypothesized that because of the noncompetitive pattern of inhibition that was observed, MPA functioned not by reversibly binding to the active site but by removing a tightly bound metal ion other than the active site cation, manganese. Further kinetic analysis using chicken mitochondrial PEPCK suggested that MPA exhibits reversible mixed inhibition.[12] The formation of a mixed disulfide E-S-S-MPA complex was hypothesized as the mechanism of inhibition and the reason for mixed inhibition but disregarded because the kinetic constants were the same in the presence and absence of a reducing agent. On the basis of the observed inhibition, it was hypothesized that the mixed inhibition could result from either partially overlapping substrate and MPA-binding sites or the fact that MPA binds at two independent sites: one affecting substrate binding and the second causing a conformational change that would be unfavorable for catalysis. The authors supported the simpler conclusion of overlapping sites but were not able to eliminate the latter possibility.[12]

Both previous kinetic studies indicated that MPA acts as a mixed inhibitor of cytosolic and mitochondrial PEPCK from rat and chicken, respectively. However, the two studies reached different conclusions about the mechanism of that inhibition. To clarify the mechanism of inhibition exerted by MPA on PEPCK, we have undertaken structural and kinetic studies of the cytosolic isozyme. These studies illustrate that PEPCK is inhibited by the binding of MPA at two discrete binding sites, one competitive with PEP/OAA and the other acting at a previously unidentified

Received: July 22, 2015
Revised: August 25, 2015
Published: August 31, 2015

DOI: 10.1021/acs.biochem.5b00822
Biochemistry 2015, 54, 5878−5887

allosteric site that stabilizes a conformation of the enzyme that is unable to bind the nucleotide substrate.

EXPERIMENTAL PROCEDURES

Glutathione Uniflow Resin was purchased from Clontech, HEPES from Research Organics, and DTT from Gold Biotechnology. GDP, GTP, ADP, and OAA were obtained from Sigma. PEP and NADH were purchased from Chem-Impex International. 3-Mercaptopicolinic acid (MPA) was purchased from Toronto Research Chemicals. HiQ, P6DG, and chelex resins were from Bio-Rad. Pyruvate kinase (PK; 10 mg/mL) was purchased from Roche. Lactate dehydrogenase (LDH) and malate dehydrogenase (MDH) were from Calzyme. All other materials were of the highest grade available.

Mutagenesis. The gene for rat cPEPCK encoding the entire 622-residue protein present in the pSUMO expression plasmid was used as the starting vector to create the C288A and R436A PEPCK variants. The forward primers (R436A, 5′-GCATCAT-TTTTGGTGGCGCTAGACCTGCAGGTGTCC-3′; C288A, 5′-GCCTTCCCCAGTGCCGCTGGGAAAACCAACCT-3′) and the respective reverse complement were utilized with the Stratagene QuikChange protocol. The resultant mutated DNA was isolated and sequenced (TCAG, Toronto, ON) in its entirety to confirm the presence of the desired mutation and the absence of any additional mutations. The plasmid DNA was subsequently transformed into chemically competent *Escherichia coli* BL-21(DE3) cells for expression.

Enzyme Expression and Purification. Rat cytosolic PEPCK was expressed in *E. coli* BL-21(DE3) cells as either a fusion protein with glutathione transferase or SUMO and purified as previously described.[13,14] In both instances, the final protein used for crystallographic and kinetic analysis was liberated from the fusion partner via proteolysis.[13,14]

Crystallization. Crystals of wild-type rat cytosolic PEPCK in complex with MPA, MPA and GTP, or MPA and oxalate were grown as previously described[15] with the following alteration. MPA dissolved in methanol was added to the drop along with GTP or oxalate, depending on the crystal complex, prior to the addition of $MnCl_2$ to obtain the desired cocrystals. Crystals of the complexes were cryoprotected in a solution containing 25% PEG 3350, 10% PEG 400, 0.1 M HEPES (pH 7.5), and 2 mM $MnCl_2$ with the addition of 1 mM MPA, 10 mM oxalate, and 10 mM GTP depending on the crystal complex. All crystals were cryocooled prior to data collection by immersion in liquid nitrogen.

Collection of Diffraction Data. Cryocooled data at 100 K on the PEPCK complexes were collected at the Stanford Synchrotron Radiation Laboratory (Menlo Park, CA), beamlines 7-1 and 11-1. All data were integrated and scaled with HKL-2000.[16] Final data statistics are listed in Table 1.

Structure Determination and Refinement. The structures of the PEPCK complexes were determined by the molecular replacement method using MOLREP[17] in the CCP4 package[18] and the previously determined rat cPEPCK structures of the holoenzyme (PDB entry 2QEW) and GTP complex (PDB entry 2QEY).[15] For each complex, the molecular replacement solution was refined using Refmac5 followed by manual model adjustment and rebuilding using COOT.[19] Ligand, metal, and water addition and validation were also performed in COOT. Final model statistics are listed in Table 1. All structural data were validated using Molprobity (http://molprobity.biochem.duke.edu),[20,21] and the statistics from this analysis are listed in Table 1.

Table 1. Crystallographic Data and Model Statistics for the Structures of PEPCK in Complex with 3-Mercaptopicolinic Acid

	PEPCK–Mn^{2+}–MPA–MPA (PDB entry 4YW8)	PEPCK–Mn^{2+}–MPA–Mn^{2+}GTP (PDB entry 4YW9)	PEPCK–Mn^{2+}–oxalate–MPA (PDB entry 4YWB)
wavelength (Å)	0.9	0.9	0.9
space group	$P2_1$	$P2_1$	$P2_1$
unit cell	a = 44.5 Å	a = 44.4 Å	a = 64.1 Å
	b = 119.4 Å	b = 118.7 Å	b = 118.7 Å
	c = 60.5 Å	c = 60.2 Å	c = 86.4 Å
	$\alpha = \gamma$ = 90.0°	$\alpha = \gamma$ = 90.0°	$\alpha = \gamma$ = 90.0°
	β = 110.2°	β = 110.0°	β = 107.3°
resolution limits (Å)	100–1.6	100–1.4	100–1.5
no. of unique reflections	83760	110377	191896
completeness[a] (%) (all data)	97.8 (84.6)	94.4 (76.2)	97.4 (83.8)
redundancy[a]	7.1 (5.0)	7.2 (5.7)	7.3 (5.8)
$I/\sigma_{(I)}$[a]	17.2 (2.0)	29.7 (3.0)	25.5 (2.3)
R_{merge}[a]	0.08 (0.49)	0.04 (0.35)	0.07 (0.47)
	Refinement		
resolution limits (Å)	29.2–1.6	29.2–1.4	27.2–1.5
no. of ASU molecules	1	1	2
R_{free}[a]	22.0 (34.4)	19.6 (37.8)	21.0 (32.7)
R_{work}[a]	18.2 (33.3)	16.9 (37.8)	17.5 (30.5)
average B factor (Å^2)			
protein (chain)			
metals (chain)	23.7	19.3	24.7 (A), 23.3 (B)
MPA (chain)	21.2	21.9	18.8 (A), 18.6 (B)
GTP	21.9	12.7	27.5 (A), 24.7 (B)
oxalate (chain)		13.4	
waters			21.1 (A), 21.4 (B)
	34.2	31.8	35.2
estimated coordinate error based on maximum likelihood (Å)	0.07	0.05	0.06
bond length root-mean-square deviation (Å)	0.02	0.01	0.02
bond angle root-mean-square deviation (deg)	1.79	1.79	1.97
Molprobity statistics (score, percentile, no. of Ramachandran outliers)	1.34, 95th, 0	1.45, 85th, 0	1.30, 95th, 0

[a]Values in parentheses represent statistics for the highest-resolution shell.

Kinetic Assays. The enzymatic activity of PEPCK was analyzed spectrophotometically by monitoring the oxidation of NADH at 340 nm at a constant temperature of 25 °C. A unit of activity is defined as the amount of enzyme forming 1 μmol of product per minute. The concentration of PEPCK was determined by its absorbance at 280 nm [ε_{280} = 1.71 (mg mL^{-1})$^{-1}$ calculated using the experimentally determined molar extinction coefficient ($\varepsilon_{280} = 1.19 \times 10^5$ M^{-1})][22] and a molecular weight of either 69416 or 69560 Da for the enzyme produced after cleavage from the SUMO or GST fusion, respectively.

The activity of PEPCK in the direction from OAA to PEP was assayed with 50 mM HEPES (pH 7.5), 10 mM DTT, 4 mM $MgCl_2$, 0.5 mM GTP, 1 mM ADP, 187.5 μM NADH, 45 units of LDH, 50 μg of PK, 0.2 mM $MnCl_2$, and (~1–2 μg) of PEPCK.

DOI: 10.1021/acs.biochem.5b00822
Biochemistry 2015, 54, 5878–5887

The assay mixture was incubated for 5 min at 25 °C and the reaction started with the addition of OAA to a final concentration of 350 μM. A second reaction without PEPCK was run simultaneously to account for the spontaneous decarboxylation of OAA. Inhibition assays with MPA were conducted under both variable OAA and variable GTP concentrations. When the GTP concentration was varied, $MgCl_2$ concentrations were also varied to keep a constant 4:1 metal:nucleotide ratio.

When the enzyme was assayed in the direction of PEP → OAA, the standard reaction mixture contained 50 mM HEPES (pH 7.5), 2 mM $MnCl_2$, 10 mM DTT, 0.5 mM GDP, 2 mM PEP, 187.5 μM NADH, 50 mM $KHCO_3$, and 11 units of MDH. The reaction proceeded at 25 °C and was started with the addition of PEPCK (~1−2 μg). Mutants were assayed as previously described with the exception that ~30 μg of enzyme was used to initiate the assay.[14] Inhibition assays with MPA were conducted with varying concentrations of PEP with a fixed GDP concentration of 500 or 25 μM. Inhibition assays against GDP were conducted at a fixed concentration of PEP of 2 or 5 mM. Assays that did not contain MPA were conducted with methanol present at the identical concentration as a blank.

Inactivation kinetic studies were performed with PEPCK that had been exchanged into 25 mM HEPES (pH 7.5) via passage over a P6DG column topped by a 1 cm bed of Chelex resin equilibrated in the same buffer to remove DTT present in the purification buffer. PEPCK (0.5 mg/mL) was subsequently incubated at 4 °C in 25 mM HEPES (pH 7.5) and either 1 mM MPA (10 mM stock in methanol) or an equivalent volume of methanol [final concentration of 10% (v/v)]. At time points between 0 and 27 h, an aliquot of the enzyme mixture was used to start the assay described above for the PEP → OAA direction.

Data Analysis. All kinetic data were analyzed using SigmaPlot11. The data at each concentration of inhibitor were fit individually to eq 1 resulting in $K_{M,app}$ and $V_{max,app}$ values. From these values, the $K_{M,app}/V_{max,app}$ ratio or $1/V_{max,app}$ was calculated, and these values were plotted as a function of inhibitor concentration and fit to eq 2 or 3 to determine the apparent K_i value.

$$\nu = \frac{V_{max,app}[S]}{K_{M,app} + [S]} \quad (1)$$

$$\frac{K_{M,app}}{V_{max,app}} = \frac{K_M}{V_{max}K_i}[I] + \frac{K_M}{V_{max}} \quad (2)$$

$$\frac{1}{V_{max,app}} = \frac{1}{V_{max}K_i}[I] + \frac{1}{V_{max}} \quad (3)$$

The rate of inactivation of PEPCK by 3-MPA in the absence of a reducing agent was determined from the slope of a plot of the natural log of the percent remaining activity as a function of time.

RESULTS AND DISCUSSION

To more completely understand the mechanism by which 3-mercaptopicolinic acid exerts its inhibitory influence upon the reaction catalyzed by PEPCK, we collected both kinetic and structural data. Together, these data suggest that the complex inhibition patterns observed for the reaction catalyzed by PEPCK are the result of MPA binding to two separate binding sites on the enzyme, one competitive with the OAA/PEP-binding site and one at a novel, allosteric site located adjacent to the mobile P-loop motif whose movement is essential for catalytic function.

Crystallography. X-ray diffraction data on three structures of PEPCK in various ligation states were collected (Table 1). The resultant structures were determined either in the presence of MPA alone (PEPCK−Mn^{2+}−MPA−MPA), in the presence of MPA and the nucleotide substrate GTP (PEPCK−Mn^{2+}−MPA−Mn^{2+}GTP), or in the presence of MPA and oxalate (PEPCK−Mn^{2+}−oxalate−MPA). Oxalate functions as a competitive inhibitor against PEP/OAA as it is thought to be a reasonable mimic of the enolate of the pyruvate intermediate formed during the reaction (K_i ~ 10 μM).[14,31] All three models are complete with the exception of amino acids composing the active site lid domain (residues ~464−471) that remains in its open/disordered conformation in all four complexes. In addition, a surface loop comprised of residues 392−397 is poorly ordered and density suitable for modeling of the region was absent from all models.

As expected from previous studies, which determined the structural requirements for small molecule inhibitors to bind at the OAA/PEP site through direct coordination to the active site manganese ion,[23] the structures of the PEPCK−Mn^{2+}−MPA−MPA and PEPCK−Mn^{2+}−MPA−Mn^{2+}GTP complexes show that MPA binds to the OAA/PEP site through direct coordination to the active site metal cation (Figure 1). MPA

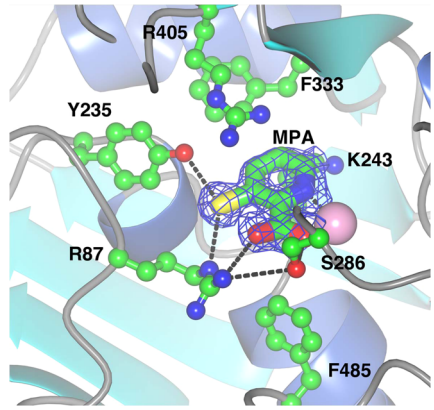

Figure 1. Binding of 3-mercaptopicolinic acid to the OAA/PEP-binding site of CPEPCK. Residues framing the binding site that are within 4 Å of the bound MPA molecule are labeled, rendered as ball-and-stick models, and colored by atom type. $F_o - F_c$ density for the inhibitor molecules rendered at 3σ prior to inclusion of MPA into the model is illustrated as a blue mesh. The dashed lines indicate potential H-bonds, and the manganese ion at the active site of PEPCK is rendered as a pink sphere.

coordinates directly to the divalent cation through the pyridine ring nitrogen and the carboxyl oxygen of the 2-carboxylate. This planar coordination geometry is seen in all ligands and/or substrates that coordinate directly to the active site manganese ion that have been structurally characterized to date.[15,23−25] In addition, the structures with MPA (PEPCK−Mn^{2+}−MPA−MPA) and MPA in complex with oxalate (PEPCK−Mn^{2+}−oxalate−MPA) demonstrate a secondary binding site (Figures 2 and 3). This binding site is located behind the active site P-loop adjacent to the well-characterized reactive cysteine residue, C288.[26−29] On the basis of the binding orientation of MPA at this secondary site, it is not surprising that the X-ray data suggest the formation of a mixed disulfide between the C-3 thiol of MPA and C288 (Figure 2). Binding of MPA to this site is not seen in the complexes of MPA with GTP (PEPCK−Mn^{2+}−MPA−Mn^{2+}GTP), suggesting that nucleotide binding and occupancy of this secondary site are mutually exclusive.

DOI: 10.1021/acs.biochem.5b00822
Biochemistry 2015, 54, 5878−5887

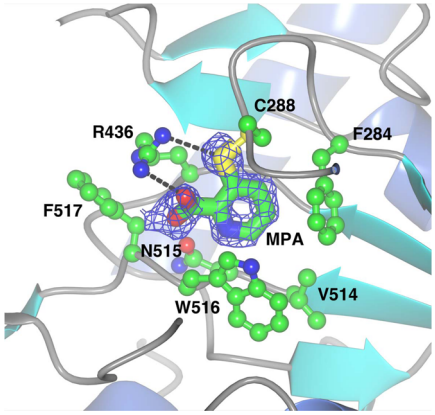

Figure 2. Allosteric site of PEPCK. The binding of MPA to the allosteric site in the presence of oxalate and MPA is illustrated. Residues framing the binding site that are within 4 Å of the bound MPA molecule are labeled, rendered as ball-and-stick models, and colored by atom type. $F_o - F_c$ density for the inhibitor molecules rendered at 2.5σ prior to inclusion of MPA into the model is illustrated as a blue mesh. The dashed lines indicate potential H-bonds.

Comparison of the PEPCK structures with MPA bound at this secondary binding site with the other structures presented here as well as previously determined structures of PEPCK deposited in the Protein Data Bank demonstrates that binding of MPA in this site stabilizes a unique conformation of the local structure. The structural data suggest that binding of MPA to this secondary (allosteric) site in the C-terminal domain of PEPCK stabilizes a more open conformation of the protein. This results in the nucleotide-binding loop adapting an open conformation. In turn, this open conformation leads to a decreased level of interaction between the phenylalanine residues that form the nucleobase-binding site, and the guanine ring of GDP/GTP. Of particular interest is the observation that the binding site for MPA sterically occludes F517 from adapting the rotomer that it typically occupies upon binding of the nucleotide (Figure 4). Evidence that interactions between the phenylalanine residues comprising the nucleobase-binding pocket and the guanine base are important in nucleotide binding affinity comes from the investigation of the affinity of ITP and GTP nucleotides, both of which can act as substrates for the PEPCK-catalyzed reaction. The available structural data suggest that the π electron system of F525 favorably interacts with the exocyclic C-2 amino group of GTP, and the binding studies confirm that the amino group contributes approximately an order of magnitude to the binding affinity of GTP as compared to ITP.[30] In addition to precluding F517 from occupying the nucleotide-bound rotomeric conformation, as described above, the structural data indicate that the allosteric binding pocket places the C-3 thiol of MPA adjacent to the thiol group of the reactive cysteine C288 that under the conditions of crystallization and/or X-ray exposure results in C288 forming a covalent mixed disulfide bond with MPA (Figure 2). Interestingly, the diffraction data on the PEPCK–Mn^{2+}–MPA–MPA complex suggest that this adduct is sensitive to exposure to X-ray radiation, resulting in the partial breakdown of the adduct and the apparent elimination of the cysteine side chain. Interestingly, no such degradation was observed at the secondary site in the presence of oxalate and MPA (PEPCK–Mn^{2+}–oxalate–MPA). Lastly, the structural studies of the oxalate–MPA complex (PEPCK–Mn^{2+}–oxalate–MPA) demonstrate that when oxalate is used to block the binding of MPA to the active site cation it is possible to occupy the allosteric site with MPA alone. Similarly, when GTP is used

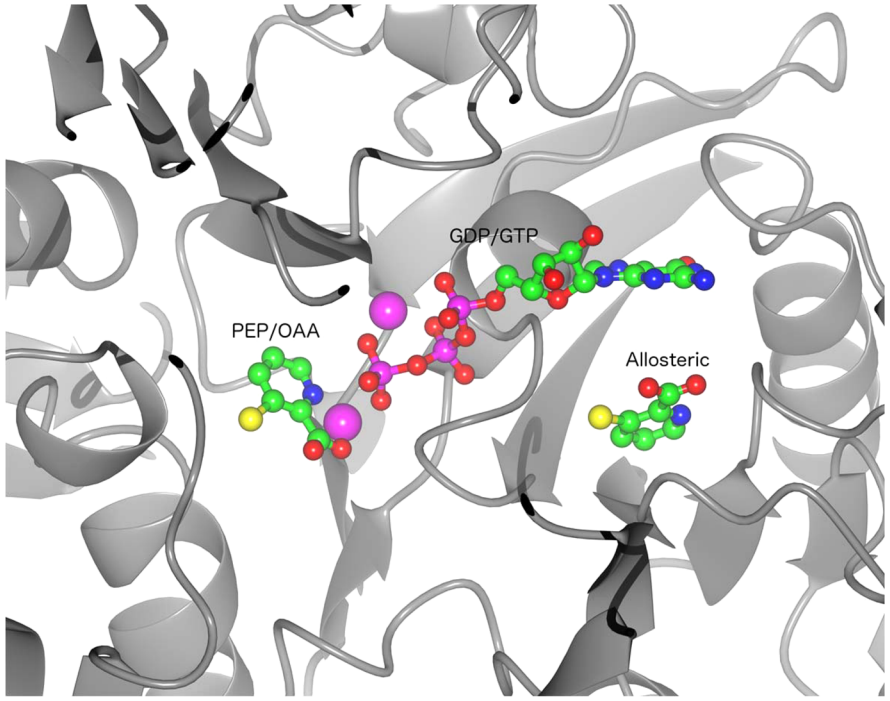

Figure 3. Location of the MPA-binding sites in relation to the active site of PEPCK. This figure was generated by the superposition of the PEPCK–Mn^{2+}–MPA–MPA and PEPCK–Mn^{2+}–MPA–Mn^{2+}GTP structures. The two binding sites for MPA, namely, the site competitive with PEP/OAA binding to the active site manganese ion and the allosteric site adjacent to the GTP-binding site, are labeled in addition to the labeling of the GTP-binding location. MPA and GTP are rendered as ball-and-stick models colored by atom type, while the active site and nucleotide-associated manganese ions are rendered as pink spheres.

DOI: 10.1021/acs.biochem.5b00822
Biochemistry 2015, 54, 5878–5887

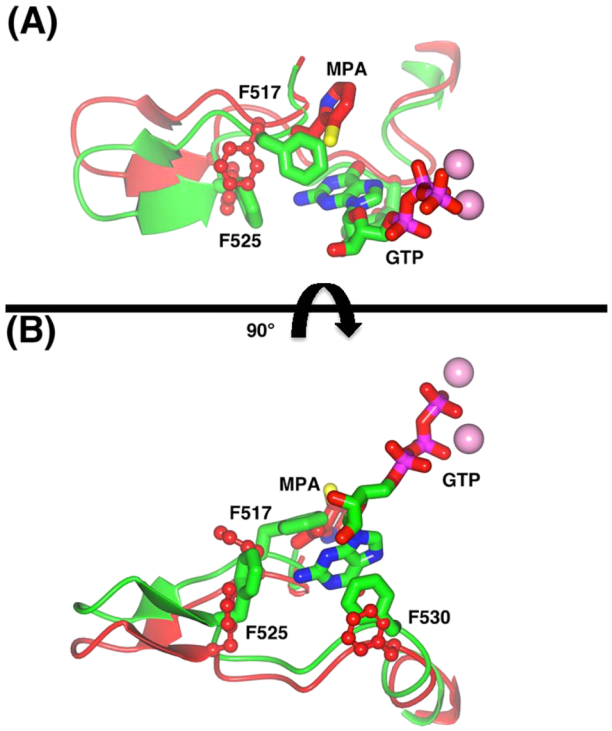

Figure 4. MPA stabilizes a form of PEPCK with a reduced nucleotide affinity. The nucleotide-binding loop (residues 515−535) is illustrated in the presence of MPA (red) or GTP (green), illustrating the different conformations of the loop stabilized by either MPA or GTP. The phenylalanine residues that make up the nucleotide-binding site are illustrated as thick sticks, labeled, and colored according to atom type. The carbon atoms (side chains, MPA, and nucleotide) are colored red or green corresponding to the coloring of the appropriate nucleotide-binding loop. The manganese ions at the active site of PEPCK are rendered as pink spheres. The view in panel B is rotated from the view in panel A about the illustrated axis by 90°.

to block binding of MPA to the secondary (allosteric) site, it is possible to singularly occupy the PEP/OAA site. Together, these data suggest that MPA can bind to each site in a manner independent of the occupancy of the other.

Kinetic Studies. *Inactivation of PEPCK.* The structural data discussed above suggest that MPA binding at the secondary binding site can covalently modify C288 through the formation of an intermolecular mixed disulfide bond. The reactivity of C288 in GTP-dependent PEPCKs has been well studied, and its modification has been demonstrated to inactivate the enzyme because of its location in the P-loop motif whose mobility is essential for catalytic function.[24,26−29,32,33] On the basis of the new structural data and the previous data suggesting that the formation of any C288 adducts inactivates PEPCK, we investigated the possibility that MPA can irreversibly inactivate PEPCK. To investigate the kinetics of C288−MPA disulfide formation, PEPCK was incubated at 4 °C in the presence of 1 mM MPA and its activity measured as a function of time. As expected, PEPCK suffers irreversible inactivation at a low but measurable rate of 0.05 h^{-1} at 4 °C (Table 2). This inactivation is prevented by the inclusion of 10 mM DTT in the incubation mix (data not shown). Further evidence that this inactivation results from the initial biding of MPA to the allosteric site and subsequent oxidation forming the mixed disulfide with C288 comes from the analysis of the inactivation of the C288A and R436A variants. When either C288, the residue involved in

Table 2. Time-Dependent Inactivation of PEPCK Variants by 1 mM MPA at 4 °C

enzyme	inactivation rate (h^{-1})
wild type	0.05 ± 0.01
wild type with 1 mM GTP	ND[a]
R436A	ND[a]
C288A	ND[a]

[a]No detectable loss of activity observed over control in the presence of 10% methanol.

mixed disulfide formation, or R436, a key residue involved in MPA recognition at the allosteric site, is mutated to alanine, neither of these enzyme forms exhibit any time-dependent loss of activity upon being incubated in the presence of 1 mM MPA (Table 2). Additionally, consistent with the structural data suggesting that nucleotide binding alters the MPA-binding site and the location of the P-loop in which C288 resides and consistent with the aforementioned prior studies of the inactivation of PEPCK via the covalent modification of C288A,[24,26−29,32,33] GTP binding protects the enzyme from inactivation by MPA modification of C288A (Table 2).

Reversible Inhibition of PEPCK. While PEPCK can be chemically inactivated by modification of C288 with MPA, the standard kinetic assay includes 10 mM DTT, and therefore, any kinetic deficit in the steady-state studies should arise from the reversible binding of MPA to PEPCK, not the formation of the intermolecular disulfide-linked adduct. In an effort to determine if both binding sites for MPA illustrated in the structural data have kinetic consequences, we conducted inhibition studies against the substrates of the reaction in both the forward and reverse directions. For all combinations of fixed and variable substrates tested, while the reciprocal plots gave patterns of lines that were suggestive of a mixed mechanism of inhibition, closer investigation suggests a more complex model that is consistent with the structural data. In this model, inhibition arises through reversible binding at two sites. One of these sites is competitive with binding of OAA/PEP to the active site cation, while the other inhibits the association of the nucleotide in a catalytically competent fashion.

OAA → PEP Direction. Upon inspection of the double-reciprocal plots generated using OAA as the variable substrate at fixed GTP concentrations, MPA appears to act as a mixed inhibitor of PEPCK, demonstrating an influence on both the slope and the intercepts of the plots (Figure 5). Replots of the primary data generate a K_i of ∼14 μM for the competitive portion of the inhibition (Figure 5 and Table 3). A weak intercept effect is also observed [K_i = 121 μM (Table 3)]. We propose that this intercept effect arises from the binding of MPA to the allosteric site of PEPCK. As cPEPCK has been suggested to obey a sequential random kinetic mechanism,[34] the [GTP]:[MPA] ratio in the kinetic assays and the relative affinities of the two ligands will dictate the amount of E-GTP available for combination with OAA to form the Michaelis complex. This results in a reduction in the observed V_{max} as a function of the MPA concentration, giving a pattern of lines in the reciprocal plot that are traditionally associated with mixed inhibition (Figure 5B).

When GTP is the variable substrate, MPA has an observable effect on V_{max} as a function of increasing MPA concentration (Figure 6). On the basis of the structural data, and the additional kinetic data in the PEP → OAA direction (below), we think it is reasonable that the V_{max} effect arises from the binding of MPA directly to the active site manganese cation in a competitive

DOI: 10.1021/acs.biochem.5b00822
Biochemistry 2015, 54, 5878−5887

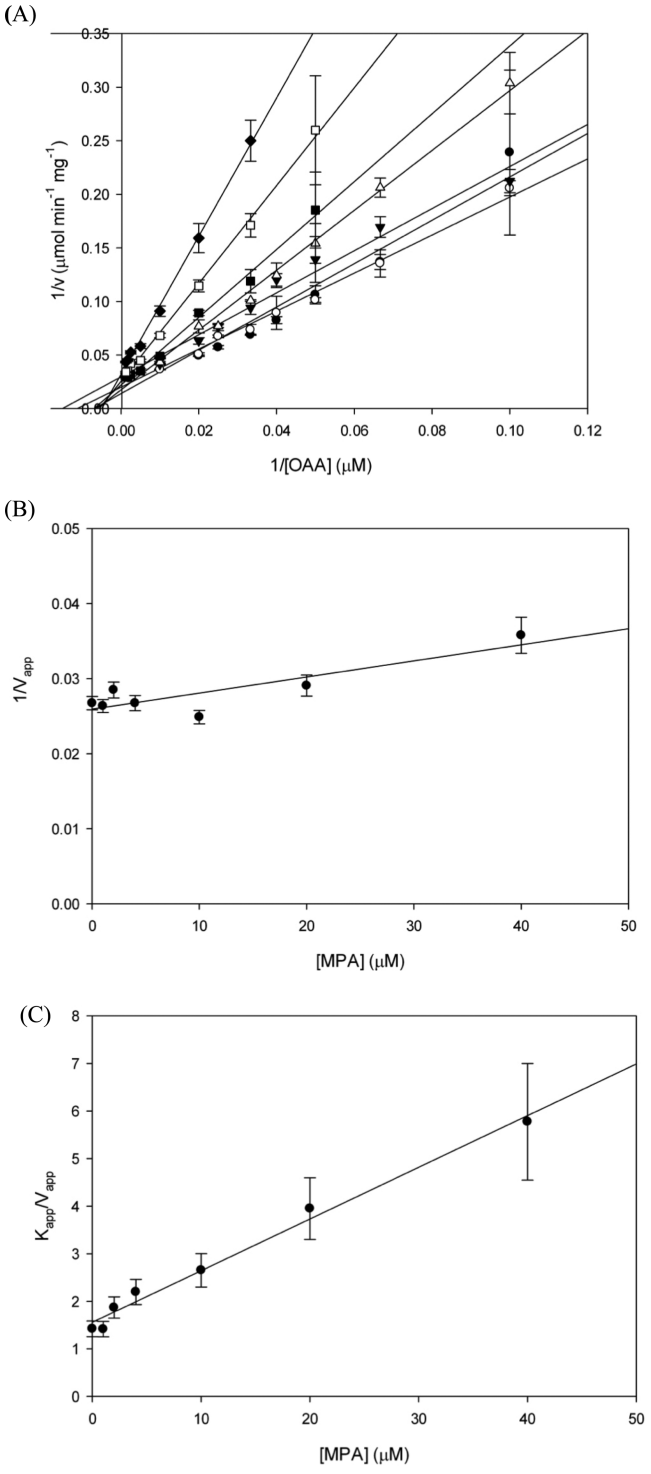

Figure 5. Inhibition of PEPCK by MPA. (A) Lineweaver−Burke plot of PEPCK activity in the direction of PEP formation with OAA concentrations variable at a fixed concentration of GTP of 500 μM. The concentrations of MPA in each plot were 0 (●), 1 (○), 2 (▼), 4 (△), 10 (■), 20 (□), and 40 μM (◆). Replot of the kinetic parameters (B) $1/V_{app}$ and (C) K_{app}/V_{app} as a function of MPA concentration.

fashion with OAA. Therefore, in the kinetic assays, as the concentration of MPA is increased, the effective concentration of E-OAA available to combine with GTP to form the Michaelis complex decreases based upon the relative affinities of OAA and MPA for the active site manganese cation of PEPCK. As GTP binds at a different site, increasing the concentration of GTP has no effect on this inhibition.

Table 3. Inhibition of WT cPEPCK by MPA at 25°C

assay direction	variable substrate	fixed substrate	kinetic parameter	K_i (μM)	attributed binding site
OAA → PEP	OA	500 μM GTP	$1/V_m$	121 ± 35	allosteric
			K_M/V_m	14 ± 2	OAA/PEP
	GTP	350 μM OAA	$1/V_m$	45 ± 5	OAA/PEP
PEP → OAA	PEP	500 μM GDP	$1/V_m$	180 ± 31	allosteric
			K_M/V_m	8 ± 1	OAA/PEP
	PEP	25 μM GDP	$1/V_m$	83 ± 7	allosteric
			K_M/V_m	5 ± 1	OAA/PEP
	GDP	5 mM PEP	$1/V_m$	83 ± 6	OAA/PEP
			K_M/V_m	362 ± 150	allosteric
	GDP	2 mM PEP	$1/V_m$	37 ± 3	OAA/PEP
			K_M/V_m	167 ± 28	allosteric

In contrast to the mixed-type pattern of inhibition when OAA was used as the variable substrate, there is no noticeable effect on K_M/V_{max} when GTP is used as the variable substrate, and in fact, the K_M for GTP is found to decrease as a function of MPA (Figure 6). At low MPA concentrations, this leads to a series of nearly parallel lines and what appears to be an inhibition pattern approximating an uncompetitive mechanism. This pattern of lines and/or mechanism of inhibition is initially confusing in light of the structural data. The structural data suggest that MPA cannot function as a true uncompetitive inhibitor because , in the presence of a saturating GTP concentration MPA binds to only the OAA/PEP site. A possible explanation for the resultant kinetic data that is consistent with the structural data is a model that proposes that GTP binds more tightly to the PEPCK−MPA complex (where MPA is bound at the OAA/PEP site) than to the PEPCK−OAA complex. This would lead to an apparent decrease in the K_M value as a function of MPA concentration because of the shifting equilibria that result from removing the E−MPA-GTP complex from the system in a fashion similar to what occurs in true uncompetitive inhibition due to removal of the ES complex by forming ESI. In addition to being consistent with the structural and kinetic data presented here, further support for this mechanism comes from two other observations. The first observation supporting the cooperativity between MPA binding at the OAA/PEP site and GTP binding is suggested by our attempts to structurally characterize a PEPCK−Mn^{2+}−MPA-Mn^{2+}GDP complex in a fashion identical to how the PEPCK−Mn^{2+}−MPA−Mn^{2+}GTP complex presented in this report was prepared. Crystals of the PEPCK−Mn^{2+}−MPA−Mn^{2+}GDP complex using commercially available GDP [containing ∼1% contamination with GTP (data not shown)] were found to continuously yield the PEPCK−Mn^{2+}−MPA−Mn^{2+}GTP complex. Thus, in the presence of MPA, the ∼0.1 mM GTP is preferentially bound over the ∼9.9 mM GDP even though the binding constants for the tri- and diphosphate nucleotides in the absence of MPA differ by a factor of ∼3.[14] Further evidence of cooperativity between inhibitor binding at the OAA-binding site and the binding of the GTP nucleotide comes from characterization of the inhibition of PEPCK by oxalate. When used as an inhibitor against OAA in the OAA → PEP direction (oxalate binding to the PEPCK−GTP complex), in our hands, the

DOI: 10.1021/acs.biochem.5b00822
Biochemistry 2015, 54, 5878−5887

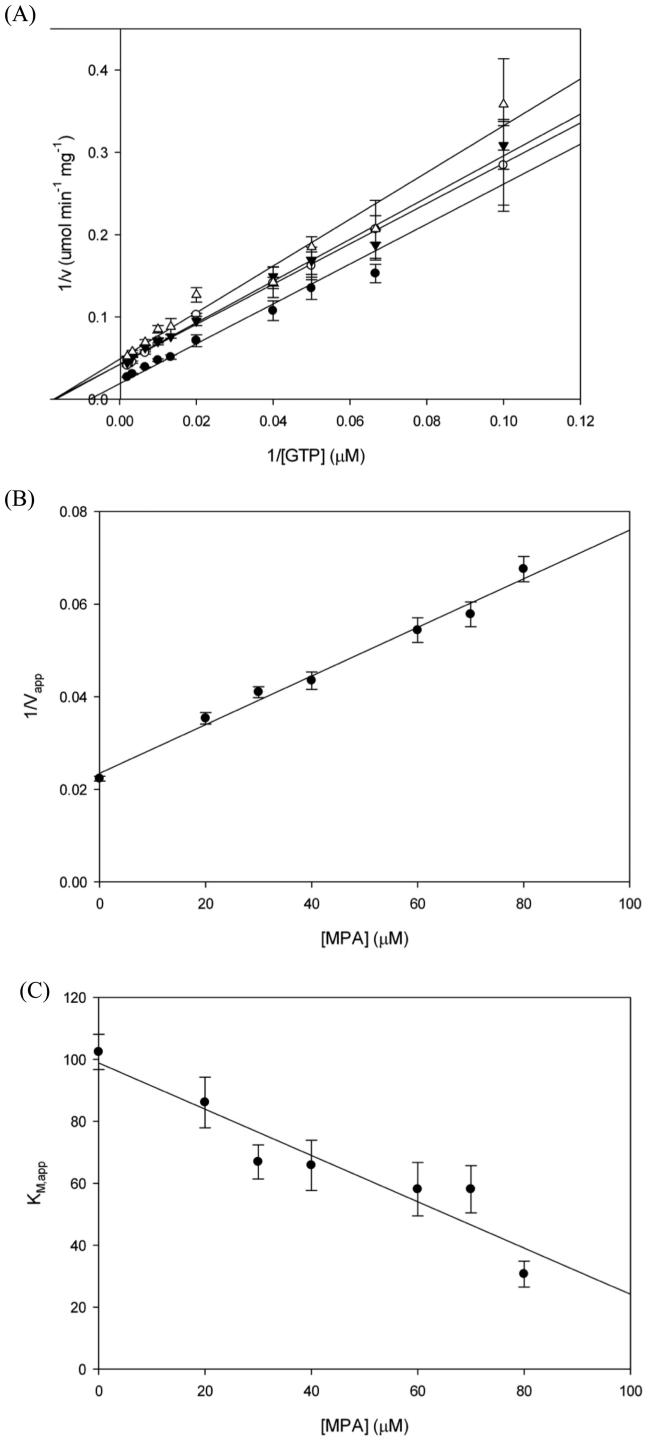

Figure 6. Inhibition of PEPCK by MPA. (A) Lineweaver–Burke plot of PEPCK activity in the direction of PEP formation with GTP concentrations variable at a fixed concentration of OAA of 350 μM. The concentrations of MPA in each plot were 0 (●), 10 (○), 20 (▼), and 30 μM (△). Replot of the kinetic parameters (B) $1/V_{app}$ and (C) K_{app} as a function of MPA concentration.

observed K_i value is ~10 μM.[14] However, in the PEP → OAA direction (oxalate binding to the PEPCK–GDP complex), its affinity is reduced by 1 order of magnitude, exhibiting a K_i of ~110 μM.[14] Lastly, because of the tight binding of GTP (K_d ~ 1 μM[30]) relative to the affinity of MPA for the allosteric site (~150 μM), MPA cannot compete with GTP over the concentration range tested (0–80 μM MPA), which we propose results in the inability of MPA to increase the $K_{M,app}$ for GTP in a competitive fashion. Therefore, the net result of these complex equilibria is an observed decrease in the $K_{M,app}$ for GTP that coupled with the reduction in V_{max} results in what appears to be a series of nearly parallel lines at low MPA concentrations and gives the illusion of uncompetitive inhibition.

PEP → OAA Direction. Similar to the inhibition pattern observed when OAA was the variable substrate (described above), at saturating concentrations of GDP, MPA appears to act as a mixed inhibitor of PEPCK (Figure 7). As outlined for the

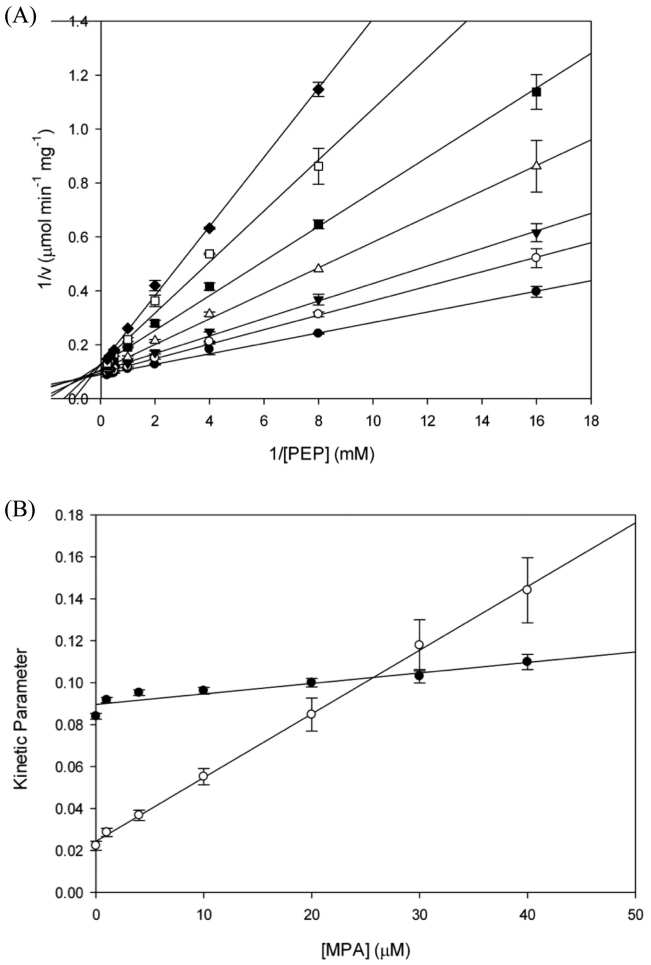

Figure 7. Inhibition of PEPCK by MPA. (A) Lineweaver–Burke plot of PEPCK activity in the direction of OAA formation with PEP concentrations variable at a fixed concentration of GDP of 500 μM. The concentrations of MPA in each plot were 0 (●), 1 (○), 4 (▼), 10 (△), 20 (■), 30 (□), and 40 μM (◆). (B) Replot of the kinetic parameters $1/V_{app}$ (●) and K_{app}/V_{app} (○) as a function of MPA concentration.

inhibition against OAA, the effect on the slope is attributed to the competition between PEP and MPA for binding to the active site metal, while the intercept effect is attributed to the binding of MPA to the allosteric site that alters nucleotide association. To further support this conclusion, we conducted additional inhibition studies at a fixed, subsaturating concentration of GDP (25 μM; K_MGDP ~ 100 μM). As shown in Figure 8, at subsaturating concentrations of GDP, the intercept shifts further from the Y-axis and the apparent K_i decreases, by ~50% (Table 3). Consistent with our mechanism of inhibition, these data suggest that the intercept effect is indeed due to the relative

DOI: 10.1021/acs.biochem.5b00822
Biochemistry 2015, 54, 5878–5887

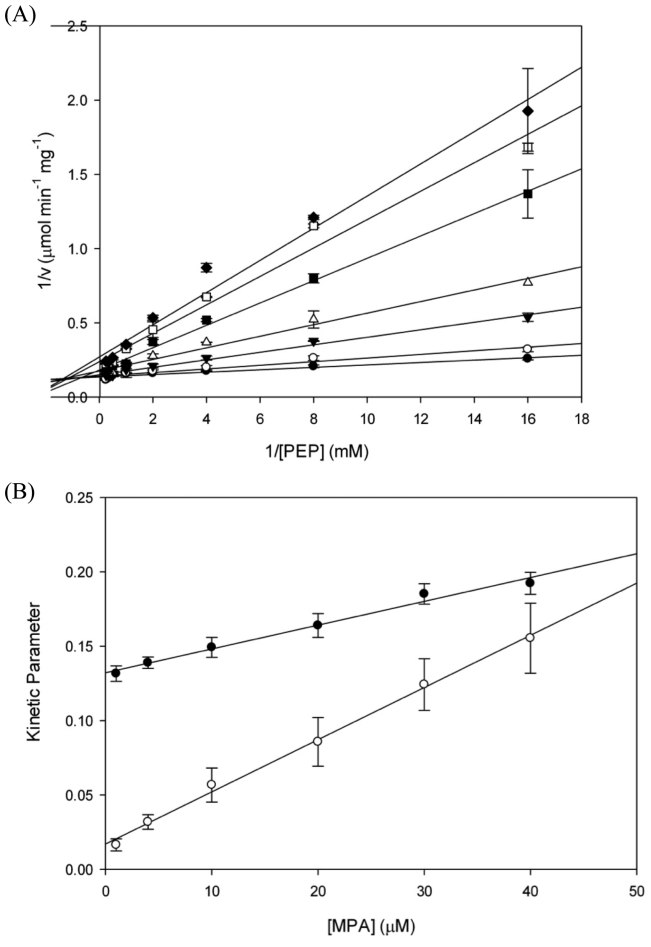

Figure 8. Inhibition of PEPCK by MPA. (A) Lineweaver–Burke plot of PEPCK activity in the direction of OAA formation with PEP concentrations variable at a fixed concentration of GDP of 25 μM. The concentrations of MPA in each plot were 0 (●), 1 (○), 4 (▼), 10 (△), 20 (■), 30 (□), and 40 μM (◆). (B) Replot of the kinetic parameters $1/V_{app}$ (●) and K_{app}/V_{app} (○) as a function of MPA concentration.

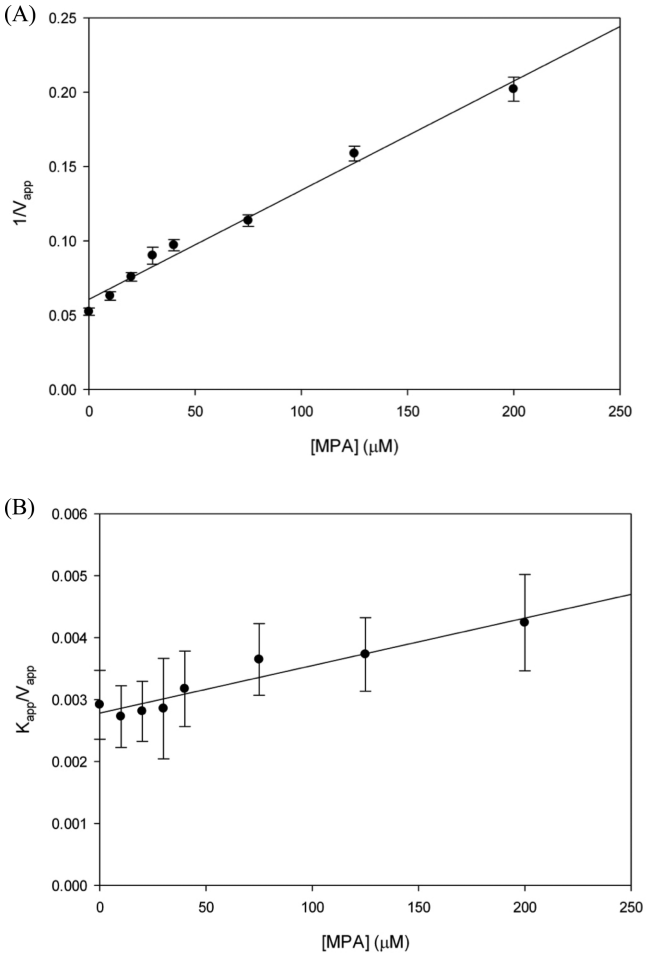

Figure 9. Inhibition of PEPCK by MPA. Plot of the kinetic parameters (A) $1/V_{app}$ and (B) K_{app}/V_{app} as a function of MPA concentration. Kinetic parameters were determined from the primary kinetic plots in the direction of OAA formation with GDP concentrations variable at a fixed concentration of PEP of 5 mM.

affinities of GDP and MPA for the nucleotide-binding sites and allosteric binding sites, respectively.

In a similar fashion, inhibition studies against GDP were conducted at fixed concentration of PEP of both 2 and 5 mM (Figures 9 and 10). These data are again consistent with the inhibition resulting from binding of MPA to two sites as suggested by the structural data. At each concentration of nucleotide, the K_i arising from the slope effect is attributed to the competition between MPA and PEP for the OAA/PEP site, and thus, the apparent K_i increases when the fixed PEP concentration is increased from 2 to 5 mM (Table 3). On the basis of our model, one would expect that the inhibition resulting from the binding of MPA to the allosteric site would be unchanged at 2 and 5 mM PEP. The data, however, indicate a change by a factor of approximately 2. The significance of the observed change is difficult to interpret based upon the error associated with the two K_i values (Table 3). The error associated with these values is partly associated with our inability to obtain data at higher concentrations of MPA because of the decrease in activity as a result of the binding of MPA to the OAA/PEP site and the relatively weaker binding to the GDP site (Figures 9 and 10 and Table 3). Despite this potential inconsistency in the observed data, we think that when the kinetic and structural data are taken as a whole, the model of inhibition proposed is consistent with the data presented.

Kinetic Analysis of C288A and R436A PEPCK Variants. To further support the conclusions reached from the structural and kinetic data, we conducted mutagenesis of the PEPCK gene to generate the C288A and R436A variants of the enzyme. Consistent with the model presented above, these mutants, which lack key elements in forming the allosteric binding pocket, demonstrate a pattern of competitive inhibition with K_i values for binding of MPA to the OAA/PEP site of 15 and 26 μM for the C288A and R436A variants, respectively (Table 4).

CONCLUSIONS

On the basis of previous crystallographic and kinetic studies, it is not surprising to find MPA coordinating directly to the active site manganese ion through its pyridinium nitrogen and exocylic C-2 carboxylate group. Similar to oxalate, and other compounds that coordinate directly to the active site manganese ion, the kinetic studies demonstrate that MPA binds tightly to the enzyme with a K_i of approximately 10 μM. While the positioning of the C288 thiol at the allosteric site allows the opportunity for a mixed disulfide to form, leading to enzyme inactivation, the data suggest that reversible binding at a second, allosteric site is the likely origin of the complex inhibition patterns observed in the kinetic

DOI: 10.1021/acs.biochem.5b00822
Biochemistry 2015, 54, 5878–5887

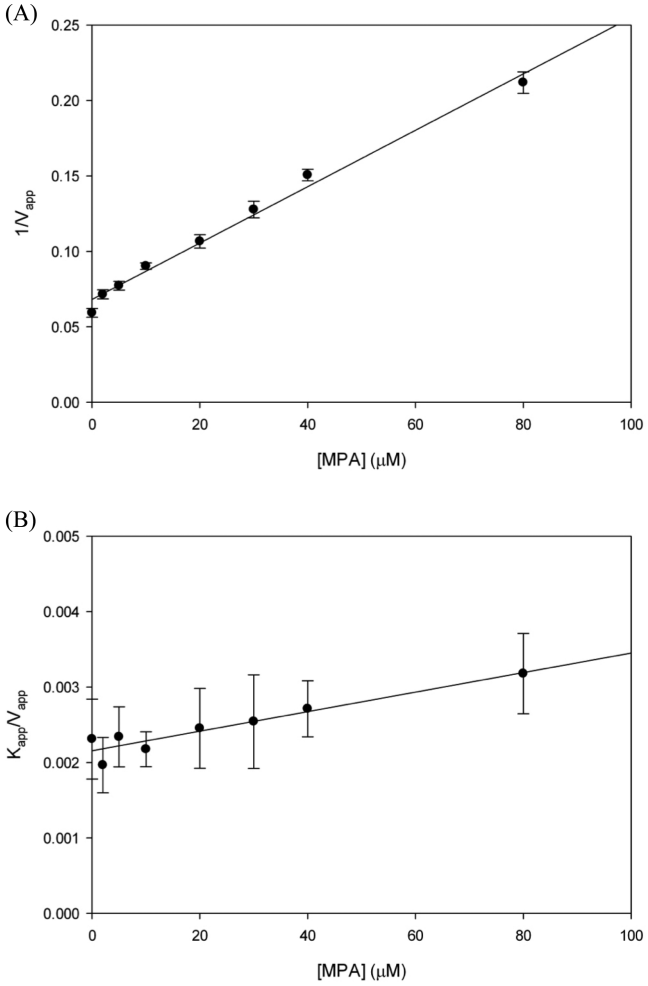

Figure 10. Inhibition of PEPCK by MPA. Plot of the kinetic parameters (A) $1/V_{app}$ and (B) K_{app}/V_{app} as a function of MPA concentration. Kinetic parameters were determined from the primary kinetic plots in the direction of OAA formation with GDP concentrations variable at a fixed concentration of PEP of 2 mM.

Table 4. Inhibition of R436A and C288A Variants of cPEPCK by MPA at 25 °C

enzyme	variable substrate	fixed substrate	kinetic parameter	K_i (μM)	mechanism of inhibition
R436A	PEP	2 mM GDP	K_M/V_m	26 ± 4	competitive
C288A	PEP	2 mM GDP	K_M/V_m	15 ± 4	competitive

studies. When taken as a whole, we think that the kinetic and structural data are consistent with a model in which cytosolic, GTP-dependent PEPCK contains a previously unappreciated allosteric site and that MPA can reversibly bind to this site and by doing so modulates PEPCK activity by affecting the ability of nucleotide to associate in a catalytically competent manner.

While binding to the allosteric site of PEPCK is modest, its identification presents the first observation that a GTP-dependent, monomeric PEPCK can be allosterically regulated. Further, this work suggests the possibility that this site could be exploited in the development of novel isozyme selective inhibitors of PEPCK and also presents the question of whether this site has any biological implications in the modulation of PEPCK activity *in vivo*.

The independent binding of MPA to two different sites on PEPCK, both of which lead to enzyme inhibition, coupled with an apparent difference in binding affinity for the two sites of approximately 1 order of magnitude complicates the interpretation of the resultant inhibition patterns. In the absence of structural data, this complexity likely led to the difficulties in assessing the mechanism of inhibition in the two previous kinetic studies.[11,12] Depending on the concentration of the fixed substrate and the concentration of the inhibitor, the patterns of inhibition can appear to shift among competitive, mixed, and uncompetitive. Interpretation of the data in the case of a multisubstrate enzyme like PEPCK is further complicated as the pattern of inhibition exhibited depends upon the nature of the variable substrate, the concentration of the fixed substrate, the concentration of the inhibitor, and the relative affinity of the enzyme for the substrates and inhibitor.

■ ASSOCIATED CONTENT

Accession Codes

Coordinates and structure factors have been deposited in the RCSB Protein Data Bank as entries 4YW8, 4YW9, 4YWB, and 4YWD.

■ AUTHOR INFORMATION

Corresponding Author

*Department of Biology, University of Waterloo, Waterloo, ON N2L 3G1, Canada. Telephone: 519-888-4567, ext. 31565. E-mail: todd.holyoak@uwaterloo.ca.

Present Address

§M.D.B.: Sanofi-Pasteur, Toronto, ON, Canada.

Funding

T.H. acknowledges support from National Center for Research Resources Grant P20 RR17708 and the Natural Sciences and Engineering Research Council of Canada.

Notes

The authors declare no competing financial interest.

■ ACKNOWLEDGMENTS

Portions of this research were conducted at the Stanford Synchrotron Radiation Laboratory, a national user facility operated by Stanford University on behalf of the U.S. Department of Energy, Office of Basic Energy Sciences. The SSRL Structural Molecular Biology Program is supported by the Department of Energy, Office of Biological and Environmental Research, and by the National Institutes of Health, National Center for Research Resources, Biomedical Technology Program, and the National Institute of General Medical Sciences.

■ ABBREVIATIONS

ADP, adenosine 5′-diphosphate; ASU, asymmetric unit; cPEPCK, cytosolic phosphoenolpyruvate carboxykinase; DTT, dithiothreitol; GDP, guanosine 5′-diphosphate; GTP, guanosine 5′-triphosphate; MPA, 3-mercaptopicolinic acid; OAA, oxaloacetic acid; PDB, Protein Data Bank; PEG, polyethylene glycol; PEP, phosphoenolpyruvate; PEPCK, phosphoenolpyruvate carboxykinase; SUMO, small ubiquitin-like modifier; TLS, translation/libration/screw; WT, wild type.

■ REFERENCES

(1) Rognstad, R. (1979) Rate-limiting steps in metabolic pathways. *J. Biol. Chem. 254*, 1875−1878.

DOI: 10.1021/acs.biochem.5b00822
Biochemistry 2015, 54, 5878−5887

(2) Hakimi, P., Yang, J., Casadesus, G., Massillon, D., Tolentino-Silva, F., Nye, C. K., Cabrera, M. E., Hagen, D. R., Utter, C. B., Baghdy, Y., Johnson, D. H., Wilson, D. L., Kirwan, J. P., Kalhan, S. C., and Hanson, R. W. (2007) Overexpression of the cytosolic form of phosphoenolpyruvate carboxykinase (GTP) in skeletal muscle repatterns energy metabolism in the mouse. *J. Biol. Chem. 282*, 32844−32855.
(3) Hanson, R. W., and Hakimi, P. (2008) Born to run; the story of the PEPCK-Cmus mouse. *Biochimie 90*, 838−842.
(4) Yang, J., Kalhan, S. C., and Hanson, R. W. (2009) What is the metabolic role of phosphoenolpyruvate carboxykinase? *J. Biol. Chem. 284*, 27025−27029.
(5) Stark, R., Pasquel, F., Turcu, A., Pongratz, R. L., Roden, M., Cline, G. W., Shulman, G. I., and Kibbey, R. G. (2009) Phosphoenolpyruvate cycling via mitochondrial phosphoenolpyruvate carboxykinase links anaplerosis and mitochondrial GTP with insulin secretion. *J. Biol. Chem. 284*, 26578−26590.
(6) Marrero, J., Rhee, K. Y., Schnappinger, D., Pethe, K., and Ehrt, S. (2010) Gluconeogenic carbon flow of tricarboxylic acid cycle intermediates is critical for Mycobacterium tuberculosis to establish and maintain infection. *Proc. Natl. Acad. Sci. U. S. A. 107*, 9819−9824.
(7) Ray, P. D., Foster, D. O., and Lardy, H. A. (1966) Paths of Carbon in Gluconeogenesis and Lipogenesis 0.4. Inhibition by L-Tryptophan of Hepatic Gluconeogenesis at Level of Phosphoenolpyruvate Formation. *J. Biol. Chem. 241*, 3904−3908.
(8) Robinson, B. H., and Oei, J. (1975) 3-Mercaptopicolinic Acid, a Preferential Inhibitor of Cytosolic Phosphoenolpyruvate Carboxykinase. *FEBS Lett. 58*, 12−15.
(9) Snoke, R. E., Johnston, J. B., and Lardy, H. A. (1971) Response of Phosphopyruvate Carboxylase to Tryptophan Metabolites and Metal Ions. *Eur. J. Biochem. 24*, 342−346.
(10) Veneziale, C. M., Walter, P., Kneer, N., and Lardy, H. A. (1967) Influence of L-Tryptophan and Its Metabolites on Gluconeogenesis in Isolated Perfused Liver. *Biochemistry 6*, 2129−2138.
(11) Jomainbaum, M., Schramm, V. L., and Hanson, R. W. (1976) Mechanism of 3-Mercaptopicolinic Acid Inhibition of Hepatic Phosphoenolpyruvate Carboxykinase (Gtp). *J. Biol. Chem. 251*, 37−44.
(12) Makinen, A. L., and Nowak, T. (1983) 3-Mercaptopicolinate. A reversible active site inhibitor of avian liver phosphoenolpyruvate carboxykinase. *J. Biol. Chem. 258*, 11654−11662.
(13) Johnson, T. A., and Holyoak, T. (2010) Increasing the conformational entropy of the Omega-loop lid domain in phosphoenolpyruvate carboxykinase impairs catalysis and decreases catalytic fidelity. *Biochemistry 49*, 5176−5187.
(14) Johnson, T. A., and Holyoak, T. (2012) The Omega-loop lid domain of phosphoenolpyruvate carboxykinase is essential for catalytic function. *Biochemistry 51*, 9547−9559.
(15) Sullivan, S. M., and Holyoak, T. (2007) Structures of rat cytosolic PEPCK: Insight into the mechanism of phosphorylation and decarboxylation of oxaloacetic acid. *Biochemistry 46*, 10078−10088.
(16) Otwinowski, Z., and Minor, W. (1997) Processing of X-ray Diffraction Data Collected in Oscillation Mode. *Methods Enzymol. 276*, 307−326.
(17) Vagin, A., and Teplyakov, A. (1997) MOLREP: an automated program for molecular replacement. *J. Appl. Crystallogr. 30*, 1022−1025.
(18) Bailey, S. (1994) The Ccp4 Suite - Programs for Protein Crystallography. *Acta Crystallogr., Sect. D: Biol. Crystallogr. D50*, 760−763.
(19) Emsley, P., and Cowtan, K. (2004) Coot: model-building tools for molecular graphics. *Acta Crystallogr., Sect. D: Biol. Crystallogr. D60*, 2126−2132.
(20) Chen, V. B., Arendall, W. B., 3rd, Headd, J. J., Keedy, D. A., Immormino, R. M., Kapral, G. J., Murray, L. W., Richardson, J. S., and Richardson, D. C. (2010) MolProbity: all-atom structure validation for macromolecular crystallography. *Acta Crystallogr., Sect. D: Biol. Crystallogr. 66*, 12−21.
(21) Davis, I. W., Leaver-Fay, A., Chen, V. B., Block, J. N., Kapral, G. J., Wang, X., Murray, L. W., Arendall, W. B., 3rd, Snoeyink, J., Richardson, J. S., and Richardson, D. C. (2007) MolProbity: all-atom contacts and structure validation for proteins and nucleic acids. *Nucleic Acids Res. 35*, W375−383.
(22) Colombo, G., Carlson, G. M., and Lardy, H. A. (1978) Phosphoenolpyruvate carboxykinase (guanosine triphosphate) from rat liver cytosol. Separation of homogeneous forms of the enzyme with high and low activity by chromatography on agarose-hexane-guanosine triphosphate. *Biochemistry 17*, 5321−5329.
(23) Stiffin, R. M., Sullivan, S. M., Carlson, G. M., and Holyoak, T. (2008) Differential inhibition of cytosolic PEPCK by substrate analogues. Kinetic and structural characterization of inhibitor recognition. *Biochemistry 47*, 2099−2109.
(24) Carlson, G. M., and Holyoak, T. (2009) Structural insights into the mechanism of phosphoenolpyruvate carboxykinase catalysis. *J. Biol. Chem. 284*, 27037−27041.
(25) Sullivan, S. M., and Holyoak, T. (2008) Enzymes with lid-gated active sites must operate by an induced fit mechanism instead of conformational selection. *Proc. Natl. Acad. Sci. U. S. A. 105*, 13829−13834.
(26) Carlson, G. M., Colombo, G., and Lardy, H. A. (1978) A vicinal dithiol containing an essential cysteine in phosphoenolpyruvate carboxykinase (guanosine triphosphate) from cytosol of rat liver. *Biochemistry 17*, 5329−5338.
(27) Lewis, C. T., Haley, B. E., and Carlson, G. M. (1989) Formation of an intramolecular cystine disulfide during the reaction of 8-azidoguanosine 5′-triphosphate with cytosolic phosphoenolpyruvate carboxykinase (GTP) causes inactivation without photolabeling. *Biochemistry 28*, 9248−9255.
(28) Lewis, C. T., Seyer, J. M., and Carlson, G. M. (1989) Cysteine 288: an essential hyperreactive thiol of cytosolic phosphoenolpyruvate carboxykinase (GTP). *J. Biol. Chem. 264*, 27−33.
(29) Makinen, A. L., and Nowak, T. (1989) A reactive cysteine in avian liver phosphoenolpyruvate carboxykinase. *J. Biol. Chem. 264*, 12148−12157.
(30) Dunten, P., Belunis, C., Crowther, R., Hollfelder, K., Kammlott, U., Levin, W., Michel, H., Ramsey, G. B., Swain, A., Weber, D., and Wertheimer, S. J. (2002) Crystal structure of human cytosolic phosphoenolpyruvate carboxykinase reveals a new GTP-binding site. *J. Mol. Biol. 316*, 257−264.
(31) Ash, D. E., Emig, F. A., Chowdhury, S. A., Satoh, Y., and Schramm, V. L. (1990) Mammalian and Avian Liver Phosphoenolpyruvate Carboxykinase - Alternate Substrates and Inhibition by Analogs of Oxaloacetate. *J. Biol. Chem. 265*, 7377−7384.
(32) Holyoak, T., Sullivan, S. M., and Nowak, T. (2006) Structural Insights into the Mechanism of PEPCK Catalysis. *Biochemistry 45*, 8254−8263.
(33) Rios, S. E., and Nowak, T. (2002) Role of cysteine 306 in the catalytic mechanism of Ascaris suum phosphoenolpyruvate carboxykinase. *Arch. Biochem. Biophys. 404*, 25−37.
(34) Jomainbaum, M., and Schramm, V. L. (1978) Kinetic Mechanism of Phosphoenolpyruvate Carboxykinase (Gtp) from Rat-Liver Cytosol - Product Inhibition, Isotope Exchange at Equilibrium, and Partial Reactions. *J. Biol. Chem. 253*, 3648−3659.

DOI: 10.1021/acs.biochem.5b00822
Biochemistry 2015, 54, 5878−5887